Nanoscale

PAPER

View Article Online
View Journal

Cite this: DOI: 10.1039/d6nr00519e

Real-time monitoring of protein–liposome interaction kinetics using absorption, polarized intrinsic emission, and scattering (APIES): insights into protein corona formation

Huajie F. Wang and Alan G. Ryder *

Liposome stability is strongly influenced by rapid protein adsorption once they enter biological environments. This dynamic "protein corona" alters membrane properties, permeability, and circulation behaviour. The early stages of protein–liposome interactions and the specific processes involved are not often studied. Addressing this gap, we report the first application of simultaneous absorption, polarized intrinsic emission (280 nm excitation), and scattering (APIES) spectroscopy with rapid mixing to monitor in real time, with second-level resolution the interaction of Human serum albumin (HSA) with 1,2-dimyristoyl-*sn*-*glycero*-3-phosphocholine (DMPC) liposomes (D_h ~150–160 nm) in ammonium bicarbonate buffer of varying ionic strength (25 to 150 mM). Dynamic light scattering (DLS) and nanoparticle tracking analysis (NTA) were used to measure changes in particle size distribution (PSD). APIES clearly showed a three-phase interaction process: first rapid (0–200 seconds) protein adsorption without penetration and osmotic pressure induced size decrease (~5 to 10%); second, a penetration phase (up to ~30 minutes) where HSA enters the lipid bilayer, and third, an annealing phase (up to 3 hours) where HSA-DMPC particle size gradually increased (by ~2 to 5%). APIES characterized the first phase by constant absorbance (*i.e.* no protein loss), minimal spectral shifts, but small reductions in emission intensity and ratio of fluorescence band area to Rayleigh–Mie scatter band area ($A_{Fl/Ry}$). Phase two displayed constant absorbance, minimal changes in $A_{Fl/Ry}$, but relatively large blue shifts (indicative of tryptophan environment changes). The final phase displayed constant absorbance, gradual increase in $A_{Fl/Ry}$ (which correlates linearly with particle size) and fluorescence intensity with minimal emission maxima changes. APIES also clearly resolved differences due to ionic strength (electrostatic screening effects) by $A_{Fl/Ry}$, (decreased by ~20% at 25 mM compared to <5% at 100–150 mM after 30 minutes) hypsochromic spectral shifts (5.9 ± 1.2 nm at 25, 3.0 ± 0.8 nm at 150 mM after 3 hours). DLS confirmed that HSA-DMPC size decreased significantly within 200 seconds after mixing, and the gradual size increase afterwards. NTA confirmed the effect of ionic strength on HSA–liposome complex size and PSD. In conclusion, APIES is a powerful, yet simple tool for monitoring protein corona formation in real time (~1 s resolution), providing more detailed mechanistic insights beyond PSD changes.

Received 6th February 2026,
Accepted 17th April 2026

DOI: 10.1039/d6nr00519e

rsc.li/nanoscale

1. Introduction

Phospholipid liposomes are potentially useful drug carriers for a wide range of substances *in vitro* and *in vivo*. However, when liposomes (or other lipid-based nanoparticles) are deployed, for example after being administered intravenously, into a real physiological environment which contains a multitude of complex biological molecules, multiple interactions ensue.[1] The most important, and immediate process is the interaction of proteins, like albumins with liposome surfaces, forming a "protein corona". This general principle, first described by Vroman in 1962,[2] suggested a time-dependent protein association and dissociation onto larger particle surface which led to the hypothesis that the "protein corona" formed is a dynamic entity that evolves over time. Therefore protein corona formed on drug carrying liposomes will influence *in vivo* behaviour particularly when injected into the bloodstream.[3] It is well documented that the physical–chemical properties of nanoparticles (NPS) are, together with the protein source, and environmental factors that shape the protein corona, particularly by, protein type and concentration,[4] solution pH,[5] and ionic strength.[6,7] Buffer systems also play a crucial role by minimizing protein aggregation while preserving liposome stability through regulation of particle size, membrane fluidity,

Nanoscale Biophotonics Laboratory, University of Galway, University Road, Galway, H91 TK33, Ireland. E-mail: alan.ryder@universityofgalway.ie; Tel: +353-91-492943

and rigidity. Increased salt concentrations have been shown to enhance bilayer rigidity, thereby stabilizing proteins in their native conformations.[8]

Components of blood plasma significantly affect liposome permeability and stability, leading to payload leakage.[1] For example, serum and some constituents induced a far more rapid (in seconds) loss of entrapped dye from phosphatidylcholine liposomes, associated with structural changes.[9] Typically, studies on the interactions between proteins and liposomes take place after incubation times of 30 minutes or more, even several days and mostly concentrate on changes in size,[10] composition,[11] or surface properties.[12] This is because it is known that complex protein coronas form quickly *e.g.* by 10 minutes after injection.[13] However, this means that the initial stages (first couple of minutes) of corona formation are generally not measured or reported on, which represents an important knowledge gap.

Binding of proteins to liposomes (and other lipid nanocarriers) reshapes bilayer structure and colloidal behaviour, often shifting size distributions as a protein corona forms.[14,15] Size changes can be monitored using Dynamic Light Scattering (DLS) and Nanoparticle tracking Analysis (NTA). DLS is non-destructive and relatively fast, but as an ensemble, intensity-weighted method, it is biased towards large particles in polydisperse samples, has poor size-resolution, and does not give a true particle size distribution (PSD). This makes it less suitable useful for the analysis of dynamic systems or where there are small changes in particle diameter for relatively large particles (*e.g.* liposomes with diameters of ~100 nm).[16,17] NTA using number-weighted tracking of individual particles, provides a more accurate and truer PSD.[18,19] Unfortunately, it usually requires sample dilution (potentially changing dynamic equilibria), requires a sufficiently high level of particle-dispersant optical contrast, and has a lower size limit of ~50 nm for biogenic particles.[20]

Previously, polarized Total Synchronous Fluorescence Scan (pTSFS) measurements were used to investigate the effect of different buffers on the interaction between human serum albumin (HSA) and DMPC (dimyristoyl-*sn*-phosphatidylcholine) liposomes.[21] Polarized excitation-emission matrices (pEEM)[22] and pTSFS[23] however, when implemented on scanning based spectrometers was too slow taking (>20 seconds per single spectrum) for kinetic studies, and thus we only investigated static samples after a 3 hours incubation. Using the anisotropy resolved multi-dimensional emission spectroscopy (ARMES) data analysis method, we observed significantly different outcomes for HSA–liposome interactions between water and various buffers, but only after this 3-hour equilibrium period.[21] However, the specific influence of ionic strength on protein–liposome interaction kinetics is less well documented, particularly during the initial, dynamic phases of interaction. Being able to measure, monitor, and thus understand these interactions will improve our understanding of the *in vivo* liposome behaviour.[24]

We developed this new absorption, polarized intrinsic emission (280 nm excitation), and scattering (APIES) spectroscopy-based method to investigate the dynamic interaction between proteins and liposomes. APIES, when implemented using a multichannel detector equipped spectrometer (here an Horiba Aqualog) enables simultaneous acquisition of fluorescence emission (at one fixed excitation wavelength), the Rayleigh–Mie elastically scattered light band,[25] and light absorbance data with 1 second resolution. The elastically scattered light band which occurs at the same wavelength as the excitation, comprises of light, elastically scattered by the solvent and solute molecules (Rayleigh scattering), and light scattered by particles (Mie scattered light).[26] In the context of liposomes, proteins, or other nanoparticles >~10 nm, one can generally ignore the Rayleigh component as Mie scattering starts to dominate and increases with particle size. Furthermore, by selecting the polarisation configuration one can enhance the sensitivity for measuring light scatter by using vertical–vertical (VV) polariser orientations or reduce the scattered light contribution by using crossed polarizers, vertical–horizontal (VH) configuration.[25,27,28] This measurement capability enables real-time, simultaneous monitoring of changes in protein environment or structure (*via* the intrinsic emission) and particle size/distribution (from changes in the intensity of the Rayleigh–Mie band). This provides a more comprehensive understanding of the photophysical changes occurring during complex molecular interactions, such as the initial phases of protein–particle interactions, particle–particle interactions, or protein aggregation.[29]

Here, using a HSA and DMPC liposome model system we investigated for the first time the efficacy of APIES for real-time, label-free monitoring of the dynamic protein–particle interaction process under varying ionic strength conditions. This provided a multidimensional view of interaction processes, suitable for *in vitro* testing of lipid based nanoparticles.

2. Experimental

2.1 Materials

1,2-Dimyristoyl-*sn-glycero*-3-phosphocholine (DMPC) (850345P-200 mg, Lot no. 850345P-200 MG-B-282) were obtained from Avanti polar Lipids. HSA (A1887, lot no. SLMBM7779 V) was purchased from Sigma Aldrich. Chloroform (99%+, Extra Pure) and ethanol (99%+, Absolute, Extra Pure) were purchased from Fisher Chemicals. NH_4HCO_3 was purchased from Fisher Chemicals and used to make ammonium bicarbonate (ABC) buffers with ionic strengths of 25, 50, 100, and 150 mM with a pH of ~8.0. All materials were used as received. Ionic strengths were adjusted solely by varying the concentration of NH_4HCO_3 without the addition of NaCl or other salts. Buffer solution pH was measured using a calibrated pH meter and was adjusted to approximately pH 8.0 with dilute NH_4OH or dilute acetic acid as necessary.

2.2 Sample preparation

HSA stock solutions (5 mg mL^{-1}) were individually prepared in each ABC buffer (25, 50, 100, and 150 mM) and then filtered through a 0.2 μm membrane filter (Whatman Cat. No. 6780-

1320). All subsequent HSA samples at lower concentrations were prepared by dilution of these filtered stocks with their corresponding ABC buffers.

Approximately 7 mg of DMPC lipid power was carefully weighed out into a glass flask, and sufficient chloroform was added to dissolve and produce a 10 mg mL^{-1} solution. The organic solvent was then evaporated under reduced pressure at room temperature for about 12 hours, producing a dry, thin lipid film. The resulting lipid thin film was re-suspended in the desired ABC buffer. Large unilamellar vesicles (liposomes) were prepared *via* extrusion using an Avanti mini-extrusion kit with a heating block at 25 °C (*i.e.* above the phase transition temperature of DMPC) and 200 nm polycarbonate filters (Whatman, 800281). For each experimental condition, liposomes were diluted from their corresponding stock solution using the same ABC buffer. This method ensured consistent buffer composition, ionic strength, and pH conditions throughout all experiments. Lipid to liposome to protein ratios are calculated in (Table S1, SI).

2.3 Methods

2.3.1 APIES analysis. APIES measurements were performed using a Horiba Aqualog spectrophotometer (Horiba, Piscataway, NJ, USA) fitted with manually operated wire grid polarizers (Thorlabs),[28] a temperature-controlled single cuvette holder, and a rapid-mixing accessory (SFA-20, TgK Scientific Limited, UK). APIES data were collected with a one second exposure, with varying time intervals using a fixed excitation wavelength of 280 nm and fixed emission range of 240–800 nm with a spectral resolution of 0.41 nm. A high CCD gain and excitation/emission slit widths of 5 nm were used for all measurements. All experiments were performed at a temperature of 25 °C using an Alpha RA 8 thermostatic circulator (LAUDA, Germany).

Spectra were collected using two different polarization configurations: vertical–vertical (VV), vertical–horizontal (VH) with a buffer blank spectrum (which was automatically subtracted). *G* factor correction was not performed for these studies, so the VH measurements are regarded as quasi-perpendicular polarized. All absorbance measurements were made with vertically polarised light. A useful parameter to characterize the particle-emission changes is the fluorescence-to-Rayleigh–Mie scattering ratio ($A_{FI/Ry}$), calculated from the ratio of the fluorescence band area (290–450 nm) to the Rayleigh–Mie scattering band area (270–290 nm). This was done using the Spectragryph v1.2 software package (F. Menges, Germany) and areas were used in preference to simple maximum band intensity to minimize the effects of particle induced intensity fluctuations.

2.3.2 Particle size analysis. Particle size measurements were conducted at 25 °C using DLS with a Zetasizer Nano ZS90 (Malvern Analytical Ltd, UK), operating in 173° backscatter mode, with the sample in quartz cuvettes, and water as the dispersant. Analysis was done using both Cumulants fitting to extract the *Z*-average hydrodynamic diameter (D_h), and polydispersity index (PDI), and distribution fitting to extract more information about sample polydispersity. This was all done using the Zetasizer software V7.13. For HSA analysis, the standard protein model was used, whereas for liposome analysis, the standard general model was used. In each case 10 runs of 20 seconds duration, with six replicates were taken for each HSA and liposome starting material. For the mixtures, the standard general model was used, with single 10 second measurements, and >100 sequential measurements taken over time for each reaction.

ζ-Potential measurements were made using an Anton Parr Litesizer DLS 500 (Anton Paar GmbH, Graz, Austria) with data analysis done using the onboard Kalliope Pro. Ver. 4.4.0 software. Each sample was measured three times, with each measurement run taking 10 minutes. HSA-liposome samples were only measured after incubating for 3 hours, as this is when the samples were considered to be relatively stable.

2.4 Monitoring protein–liposome interactions

HSA and liposomes were dissolved in ABC buffer, with final concentrations, after mixing, of 1 mg mL^{-1} HSA and 0.25 mg mL^{-1} DMPC liposomes (HSA : liposome ratio = 6563 : 1 to 9615 : 1, Table S1, SI). Initially, approximately 20 mL of buffer was used to rinse the rapid mixing system to remove any residual air bubbles. This was followed by rinsing with HSA solution (2 mg mL^{-1} in buffer) to further condition the system. Then HSA (2 mg mL^{-1}) and liposome (0.5 mg mL^{-1}) solutions were separately loaded into the two drive syringes. Following removal of residual air bubbles, drive syringes were triggered simultaneously to ensure rapid solution mixing, with excess solution directed into a waste syringe. To compensate for the approximately 1.0 mL priming volume in the tubes between the drive syringes and the observation cell, each measurement was conducted after first rapidly undertaking four consecutive drive syringe injections to flush the system and taking the data directly after the fifth injection. Testing with varying numbers of injections (data not shown) showed that consistent data and optimal mixing were obtained after 4 or 5 injections.

Each protein–liposome interaction was analysed over 3 hours, with APIES data collected at various time points and intervals. APIES measurements were performed using 1 second integration times, with an interval time equal to the integration time. When the total run time was set to 50 s, each run yielded 51 data points. Thus, for the first 100 s, the measurement was conducted through two consecutive batch experiments, each lasting 50 s, under the same experimental conditions. For next 30 minutes, APIES data with 1 second exposures were collected at 1 s intervals (50 spectra). Subsequently, data were recorded at set time points: 1 hour, 1.5 hours, 2 hours, 2.5 hours, and finally at 3 hours. In each case, 50 spectra with 1 s exposure were collected, and the data was then averaged.

Every protein-buffer combination was tested independently in triplicate, on different days, using freshly prepared liposomes.

In parallel, we attempted to measure particle size changes in HSA–liposome mixtures using DLS. Samples were prepared in quartz cuvettes by adding 500 μL of HSA (2 mg mL^{-1}) followed by the rapid addition of an equal volume (500 μL) of liposomes (DMPC, 0.5 mg mL^{-1}). The mixture was thoroughly

mixed in the cuvette, inserted into the DLS system, and data collection started immediately without any equilibration time (~10 seconds between addition and measurement start). Each measurement run was of 10 seconds duration. The same time intervals as used for the APIES measurements were implemented: 0–0.5 hours (continuous 10 s DLS measurements), 30 to 60 minutes (continuous 10 s DLS measurements). For the 1.5, 2, 2.5, and 3 hours timepoints a series of 20 × 10 s measurements were made.

NTA was performed using a NanoSight Pro (Malvern Instruments, UK) with a 488 nm laser excitation with particle size being calculated from path analysis of individual particles using the Stokes–Einstein equation.[30] For the HSA–liposome mixtures, 1.0 mL HSA (2 mg mL^{-1}) was rapidly combined with 1.0 mL DMPC liposomes (0.5 mg mL^{-1}) in Eppendorf tubes, mixed thoroughly, and incubated at a constant 25 °C. Aliquots were collected at 0.5, 1.0, 1.5, 2.0, 2.5, and 3.0 h, then diluted 1 : 1000 (v/v) in buffer before injection into the NTA cell for analysis. Each measurement comprised of 5 × 11.5 seconds videos (65 frames per second), with an average of between 20 and 60 particles captured per frame.

Statistical analyses (one-way or two-way Analysis of Variance (ANOVA)) were performed using GraphPad Prism version 10 (GraphPad Software, San Diego, CA, USA) and a detailed statistical analysis section is included in section S-12 of the SI. All quantitative data are expressed as mean ± SD from three independent experiments.

3. Results and discussion

APIES using a rapid-mixing accessory was employed to monitor the kinetics of HSA–liposome interactions under different ionic strength conditions. Manual mixing within the cuvette was found to be inconsistent, producing unreliable measurements, during the first 200 seconds after mixing. Polarization enabled sensitivity to be tuned where the $PIES_{VH}$ spectral measurements minimised the contribution of Rayleigh–Mie scatter, providing a clearer and truer representation of the fluorescence emission, whereas in $PIES_{VV}$ spectra, Rayleigh–Mie scatter bands were enhanced, making this polarisation more sensitive to changes in particle size, concentration, and distribution.[31] The buffer subtraction procedure used here effectively only removes Rayleigh scatter (*i.e.* molecular light scatter) and thus the Rayleigh–Mie bands recorded should be primarily composed of Mie (*i.e.* particle) scattered light. Henceforth, when we discuss (light) scattering it refers only to Mie/particle scattering. Here, parameters such as: emission maximum (λ_{max}), emission intensity, band profile, and Rayleigh–Mie/emission ratio along with the simultaneously measured absorbance provides a more comprehensive characterisation method for these interactions at second timescales. Particle size and zeta potential analyses by DLS were conducted to provide complementary size information about the interactions.

3.1 Starting material characterization

We first characterized the size, zeta potential, and maximum emission wavelength (λ_{max}) of the liposomes (Lip.) and HSA in ABC buffer solutions with varying ionic strengths (Table 1). These parameters were selected because both electrostatic interactions[32] and hydrodynamic properties (viscosity and diffusion)[33] are known to influence the interaction process. The particle diameter (*Z*-Average) of HSA (~10 ± 1 nm) and liposomes (148 ± 8 nm to ~163 ± 10 nm) remained relatively constant as the ionic strength increased from 25 to 150 mM.

Table 1 Size and spectral characterisation data for HSA and liposomes in different buffers (25, 50, 100, and 150 mM).

Ionic strength	25 mM	50 mM	100 mM	150 mM
HSA				
Z-Average (nm)	10.3 ± 0.7	10.4 ± 0.6	10.4 ± 0.2	10.1 ± 0.1
PDI	0.29 ± 0.03	0.28 ± 0.01	0.27 ± 0.01	0.26 ± 0.02
Peak 1 (dist.) (nm)	8.7 ± 0.3	9.3 ± 1.3	9.3 ± 0.6	9.3 ± 0.7
Pk 1 area int (%)	77.1 ± 5.5	79.0 ± 5.2	79.0 ± 3.3	80.5 ± 4.3
D (μ^2 s^{-1})	48.0 ± 3.0	47.6 ± 2.5	47.4 ± 0.7	48.8 ± 0.6
Zeta potential (mV)	−15 ± 2.7	−17 ± 2.7	−14 ± 1.9	−9 ± 2.0
VV λ_{max} (nm)	333.3 ± 0.3	333.3 ± 0.1	332.5 ± 0.5	333.4 ± 0.2
VH λ_{max} (nm)	335.1 ± 0.3	334.8 ± 0.4	335.0 ± 0.2	335.1 ± 0.3
Liposomes				
Z-Av. (nm)	150 ± 5	156 ± 10	148 ± 8	163 ± 5
PDI	0.12 ± 0.01	0.11 ± 0.01	0.11 ± 0.01	0.11 ± 0.02
Peak 1 (dist.) (nm)	173 ± 7	178 ± 12	169 ± 9	184 ± 4
Pk 1 area int (%)	100.0 ± 0.0	100.0 ± 0.0	100.0 ± 0.0	100.0 ± 0.0
D (μ^2 s^{-1})	3.3 ± 0.1	3.2 ± 0.2	3.3 ± 0.2	3.0 ± 0.1
Zeta potential (mV)	−2 ± 0.6	0.7 ± 0.8	2.4 ± 0.9	2.3 ± 0.2

The diameter (*Z*-Av., nm), PDI, peak 1(nm), Pk 1 area intensity present % (peak 1 area int), *D* (μ^2 s^{-1}), zeta potential (mV), and maximum emission wavelengths (λ_{max}) under vertical–vertical (VV) and vertical–horizontal (VH) polarisation configurations. Data is presented as mean ± standard deviation (n = 3 days). The liposome size variability (reported as the standard deviation of replicate runs is attributed to batch-to-batch differences arising from independent liposome preparations). For each set of experiments, liposomes were freshly prepared on three separate days.

Nanoparticle tracking analysis (NTA) confirmed this as there was no significant change in liposome size distribution with ionic strength (Fig. 6A, *vide infra*). HSA polydispersity (PDI) marginally decreased with increasing ionic strength, from 0.29 ± 0.03 to 0.26 ± 0.02, whereas liposome PDIs were consistently low (~0.1) for all buffer conditions. The higher HSA polydispersity indicated the presence of some oligomers or aggregates, and thus distribution fitting of the DLS data was needed (Fig. S1 & S2, SI). This was due to the fact that the Cumulants fitting that produces the *Z*-average parameter generates this single averaged size that represents the whole particle population, but this is biased by larger particles due to the intensity-weighting nature of DLS.[34] This results in irregular fits for polydisperse samples and thus it is a less accurate parameter for tracking size changes in complex samples.

Intensity distribution fitting of the same DLS data (Table 1) showed that the effect of ionic strength on them was relatively small. Here, peak 1 was the small species present and changes in the relative area of this peak was a good diagnostic of the degree of aggregation. For HSA, peak 1 size and area did not change significantly (all within limits of error) as ionic strength increased. DMPC liposomes were all monodisperse and there was a slight increase in size with ionic strength: distribution fit, peak 1 from ≈169 to 184 nm (which was not statistically significant, $p > 0.05$, see SI for more details). For liposomes, experimental and simulation studies on PC bilayers (POPC/DPPC/DMPC-like systems) have shown salt-induced ordering/rigidification which slowed lipid diffusion, and this was consistent with size trends observed here.[35–37]

For HSA, the zeta potential remained approximately constant between 25 and 100 mM and became less negative at 150 mM under our experimental conditions (pH ~8.0) (Table 1). This can be attributed to the screening of surface charge density, because HSA is negatively charged with an isoelectric point (PI) of ~4.8.[38] For liposomes, zeta potential increased progressively with rising ionic strength which was consistent with previous findings on zwitterionic lipid systems. These demonstrated that despite a zero net charge, PC headgroups can generate a nonzero surface potential due to their asymmetric orientation and structuring of hydration layers at membrane interfaces. Garcia-Manyes *et al.*[39] reported that DMPC vesicles exhibit a negative zeta potential in ultrapure water (−12.0 ± 1.6 mV), which gradually shifts toward positive values as ionic strength increases. It is important to note that the measured zeta potential does not directly represent the actual surface charge but is the electrostatic potential at the boundary between Stern and diffuse layers layer. Thus, it gives a useful approximation of the surface potential and is thus useful in the context of explaining the observed interactions.

For all ionic strengths, HSA emission maxima (λ_{max}) remained essentially unchanged for both polarization states, VV ≈ 333 nm; VH ≈ 335 nm (Table 1), indicating that ionic strength in this range does not measurably alter the microenvironment of HSA's single Trp (*i.e.*, no detectable change in polarity/solute–solvent relaxation around the fluorophore). VH spectra had a consistent λ_{max} red shift of ~2 nm compared to VV spectra which arises from the detection geometry in polarization-resolved measurements: the perpendicular (VH) polarisation captures emission from fluorophores that have undergone greater orientational depolarization and solvent relaxation, which are typically associated with slightly longer-wavelength emission. Such small VH > VV offsets are a well-recognized feature of fluorescence anisotropy measurements where a *G* factor instrument response has not been applied (as is the case here).[40]

3.2 Liposome–HSA interactions

To investigate the dynamic, time-dependent protein corona evolution, we used APIES data which was cross referenced with DLS measurements. Overall, APIES and DLS analyses showed that protein–liposome interactions proceeded through three kinetically distinct phases: an initial fast adsorption phase (0–200 s), a penetration phase (approximately 200–1800 s), followed by an annealing phase (1–3 h). The ratio of the emission to Rayleigh–Mie band areas ($A_{FI/Ry}$) was a particularly sensitive parameter for distinguishing subtle size-related changes whereas spectral shifts of the protein emission relate to structural and environmental changes. To compare results across different experimental conditions and eliminate variations caused by instrumental response or lamp intensity in absolute signal strength, we typically use the normalized $A_{FI/Ry}$ *ratio* where the values are scaled relative to the initial time point ($t = 0$), enabling direct comparison of relative changes over time under different conditions. Since each individual experiment used a fresh liposome preparation this resulted in slightly different sized liposomes being used for each experiment. This is a significant contributor to the error bars reported in the experiments below and should be reduced with batch manufacturing of liposomes.

3.2.1 Initial mixing and adsorption (0–200 s). Immediately after mixing, APIES data using a single 280 nm excitation wavelength and fixed polarisation (typically VV) were collected every second. As the polarizers were manually operated it required separate experiments to collect APIES data with different polarisations. For the first 50 seconds after mixing, the VV (Fig. 1A) and VH emission spectra (Fig. 1B) showed relatively little change. The big difference between the VV and VH spectra was the effect on the Rayleigh–Mie band (Fig. 1C) which was nonexistent in the VH measurement (because of the crossed polarisers), providing a cleaner emission spectrum (Fig. 1D).

In the first 200 seconds after mixing, there was a small (~5%) drop in fluorescence intensity (normalized to t_0) for both VV (Fig. 2A and Fig. S3B, SI) and VH spectra (Fig. 2B) while the emission maximum (λ_{max}) remained constant (Fig. 2C/Fig. 2D). This was accompanied by a small drop in the Rayleigh–Mie intensity of between 4 and 8% (Fig. S3A, SI). The lower emission intensity observed in the VH configuration compared to VV is expected and arises from the polarization characteristics of fluorescence emission. Under vertically polarized excitation, fluorophores are preferentially excited with their transition dipole moments aligned along the excitation polarization. As a result, the emitted fluorescence is par-

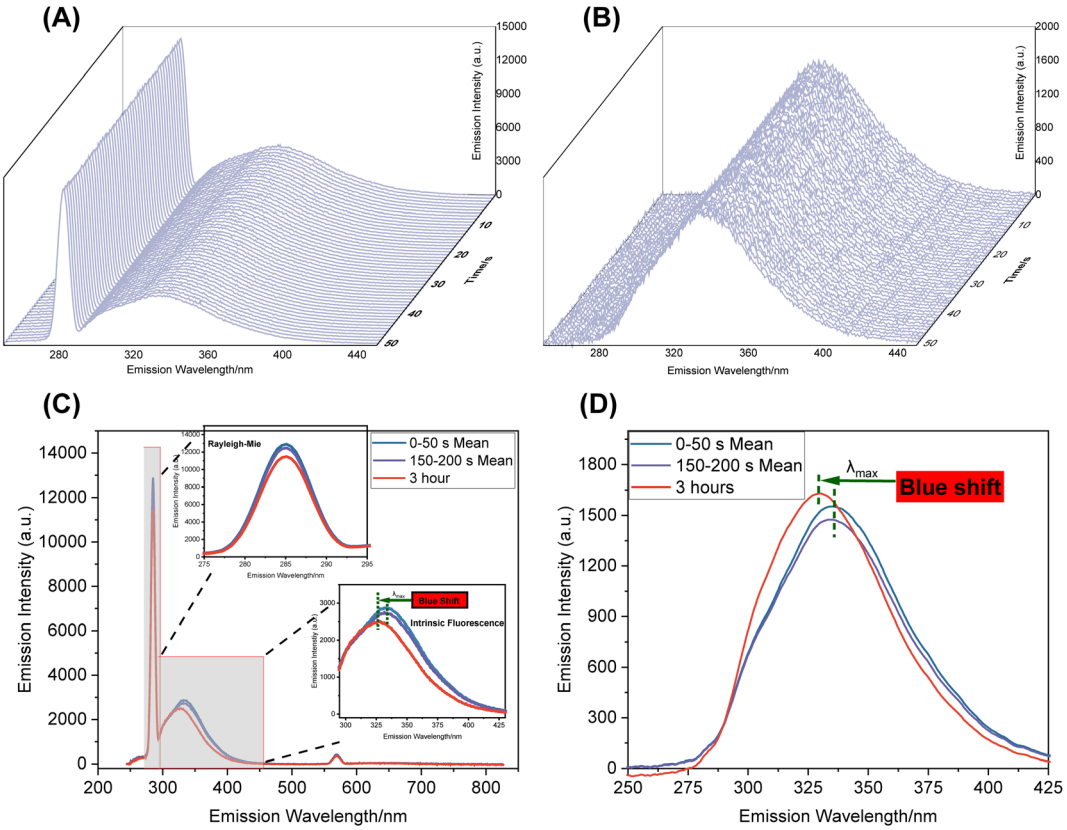

Fig. 1 APIES spectra (280 nm excitation) of HSA–liposome interactions collected during the first 50 seconds after mixing: (A) VV polarisation, $PIES_{VV}$, and (B) VH polarisation, $PIES_{VH}$; averaged PIES spectra collected over full observed interaction period: (C) $PIES_{VV}$ spectra showing Rayleigh–Mie scattering and intrinsic fluorescence and highlight blue shift of emission maxima (λ_{max}); (D) $PIES_{VH}$ spectra showing intrinsic fluorescence and time-dependent blue shifts. To show signal change evolution more clearly, we plotted the normalized fluorescence, obtained by scaling emission intensities relative to the initial intensity at t_0.

tially polarized, and the emission intensity detected parallel to the excitation polarization (VV) is generally higher than that detected in the perpendicular configuration (VH) particularly for slowly rotating large molecules or particles. In addition, Rayleigh/Mie scattering is also polarization-dependent and contributes more strongly in the VV configuration while being reduced in the VH configuration. Therefore, the observed difference between VV and VH reflects the intrinsic polarization behavior of the system rather than any differences in sample concentration.[40] Overall, this suggested that either the protein has not interacted with the liposomes, or that it was only surface-level adsorption. The absorbance at 280 nm was also monitored and this showed minimal changes during this time (Fig. 2E and Fig. S3C, SI), which suggested that all protein remained in solution or on the liposome surface and there were no significant ionic strength effects. Furthermore, the normalized $A_{FI/Ry}$ ratio (VV polarisation) did not change significantly, <4% (Fig. 2F), however, the trends were ionic strength dependent. The order of variation is different because changes in absorbance is mostly due to protein content (and a small contribution from scattered light) and thus remains relatively constant whereas $A_{FI/Ry}$ ratio reports changes in emission and light scattering which vary much more significantly because of how ionic strength affects the adsorption of protein on surfaces. The normalized $A_{FI/Ry}$ ratio gradually changed over time, decreasing to 0.97 at 25 mM and 0.99 at 50 mM, and increasing to ~1.01 at 100 mM and 150 mM, suggesting that there was some form of interaction underway that was modulated by ionic strength. We propose, and this is consistent with data below, that HSA is rapidly adsorbed onto the surface, but does not penetrate the surface. This adsorption causes emission quenching (Fig. 2A/Fig. 2B) because the HSA molecules are more concentrated on the surface, with the differences in $A_{FI/Ry}$ ratios being associated with the strength of the interaction which is affected by charge screening and dependent on ionic strength (*vide infra*).

We attempted to undertake time-resolved (10 s serial acquisitions) size measurements within the first 200 s, but these produced inaccurate size information with large errors (Fig. S4, SI). This was because of three reasons, first its poor time resolution (minimum of 10 seconds per measurement), second the need to average multiple measurements to obtain accurate size data, and third because of its limited ability to discriminate species of similar hydrodynamic size (see bimodal discussion in SI). Here, DLS does however provide one highly reliable and accurate parameter, namely the scat-

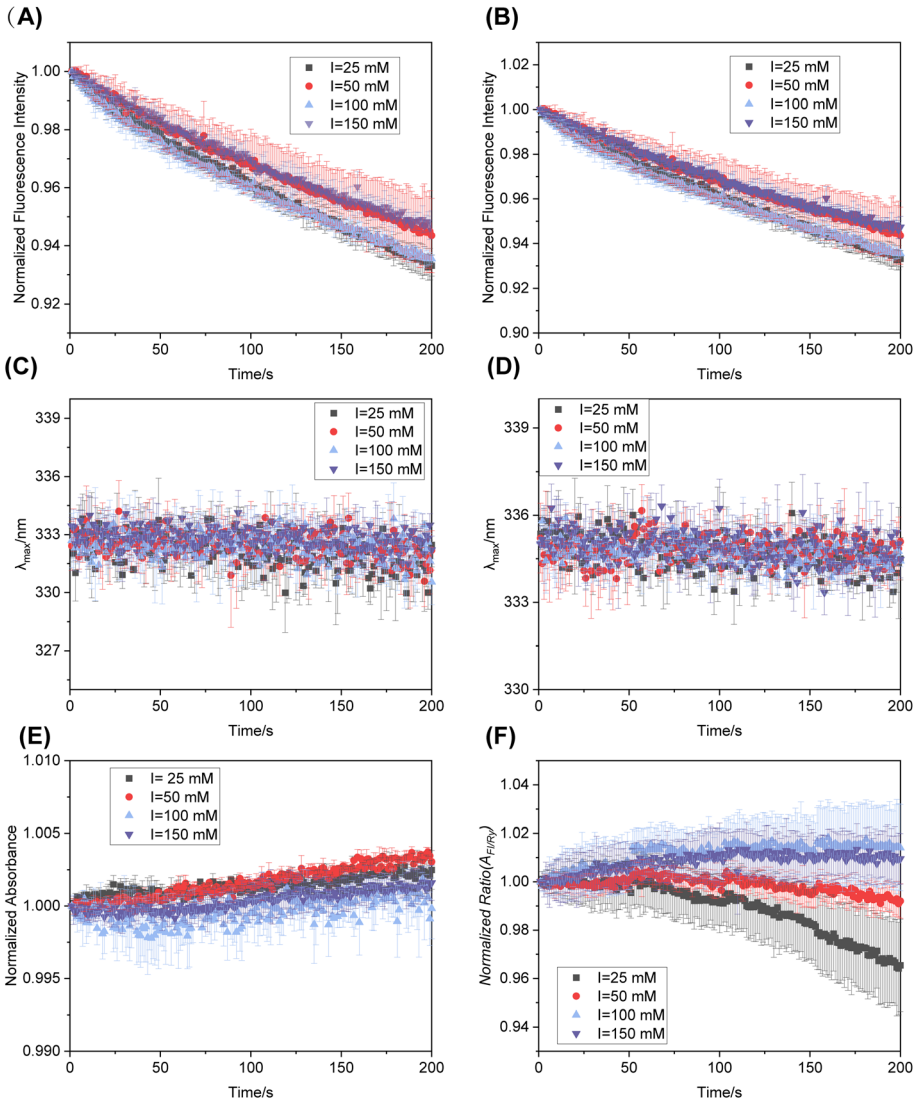

Fig. 2 Plots of changes in spectral properties *versus* time (0–200 s) after mixing HSA and liposomes under different ionic strengths: (A) normalized VV Fluorescence intensity (area under the curve); (B) normalized VH Fluorescence intensity (area under the curve); (C) emission VV maxima (λ_{max}); (D) emission VH maxima (λ_{max}); (E) normalized absorbance, and (F) normalized $A_{FI/Ry}$ ratio. See also Fig. S3, SI.

tered light intensity (Mie or particle scattered) as measured by the derived count rate (DCR). This is the signal corrected for the attenuator setting and represents an accurate measure of the real scattered light intensity at 632.8 nm which depends on both particle size and number of particles. Although DCR decreased by ~30–35% for all ionic strengths (Fig. 3A and Fig. S4A, SI), this result alone is not sufficient evidence for a reduction in the hydrodynamic size of HSA–liposome assemblies. This DCR drop also could be attributed to material loss, but here, this does not occur because the absorbance signal (which also includes a scattered light contribution from the liposomes) does not decrease. Thus, this drop in DCR is most probably due to a reduction in particle size (see also section 1.5, SI for more details).

It is also possible, but unlikely, that an optical-smoothing effect, caused by significant differences between the refractive indices of HSA and liposome could cause a reduction in light scattering. When HSA adsorbs, it forms an interfacial shell whose refractive index lies between that of the lipid bilayer and the aqueous medium. This layer smooths the refractive-index gradient at the particle–solvent boundary, reducing overall scattering efficiency without a significant change in particle size.[41] However, we have no evidence to support this since these measurement methods (DLS and APIES) are not sufficiently sensitive. It may be possible to explore this using single particle analysis techniques,[42] but that is outside the scope of this work.

The normalised (to t_0) particle size diameter (*Z*-average, Fig. 3B and Fig. S4B, SI) show a small (~10%) decrease in particle size. *Z*-Average sizes were analysed using a two-way ANOVA with ionic strength and time (t_0 *vs.* t_{200} s) as factors (Fig. S14A, SI). A statistically significant decrease in particle size was

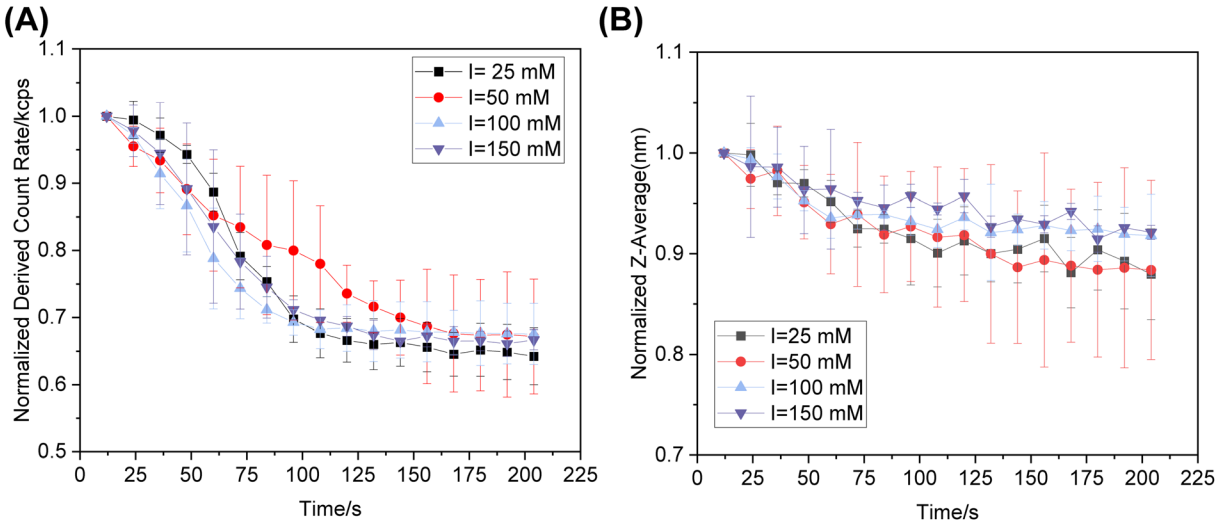

Fig. 3 Plots of DLS data from first 200 seconds after HSA Liposome mixing: (A) the normalized DCR *versus* time; and (B) normalized diameter (*Z*-average, nm) *versus* time. The data presented are the mean and standard deviations from three independent experiments for each ionic strength condition.

observed only at the lower ionic strengths (25 and 50 mM), whereas at 100 and 150 mM only a non-significant trend toward smaller particle size was observed. Although the errors were relatively large, the size decrease at lower ionic strengths was reproducible across independent measurements. Plotting the DLS measurements made over the first 1800 seconds (Fig. S5, SI) confirm that there were decreases in particle size during this initial period after mixing and that the change was larger for the low ionic strength conditions. However, the change was only statistically significant for the 50 mM case, (Fig. S15, SI). Distribution fitting of the DLS data does not improve the accuracy of the size measurements as seen in the plot of the main peak extracted from the distribution fits (peak 1) against time (Fig. S4D, SI) as the size values had large errors and scatter. Accurate DLS size measurements require much longer acquisition times and averaging of multiple measurement runs which is normally longer than the 200 s observation window here. Thus, although we cannot accurately track either liposome or protein size/contribution changes during this early phase, we can say that there is a small decrease in size. After DCR, the most reliable parameter for evaluating gross changes was the PDI which increases very significantly at all ionic strengths after mixing (Fig. S4C, SI), which is indicative of some form of protein mediated size changes or aggregation.

A particle size decrease of ~10% should result in a drop in Mie scattered light intensity of ~30% which agrees with the ~30% decrease in derived count rate at 632.8 nm (Fig. 3). However, the $A_{FI/Ry}$ ratio data only decreased by approximately 4% (at lower ionic strengths) or not at all for higher ionic strengths (the ratio remained unchanged in the first 200 s), and the Rayleigh–Mie scattered light intensity at 280 nm only decreased by ~10% (Fig. S3A, SI). We note that the Rayleigh contribution to this signal, measured using buffer blanks, is very small, typically <2%, and will remain constant. Thus, this discrepancy between the observations at 632 and 280 nm wavelengths, can be explained by the increased absorbance at 280 nm from an adsorbed protein layer which will reduce the effective scattering cross sections of the particles, resulting in much smaller changes in Mie scatter in the UV.[43]

Taken all together, these results prove that protein–liposome interactions are occurring, and although we cannot accurately measure liposome size changes by DLS during this initial period, there was a clear decrease. This unexpected, initial liposome shrinkage directly after mixing we attribute to an osmotic pressure gradient induced by HSA primarily in the surface bound layer and secondly in the surrounding buffer. Elevated protein concentrations in the bound layer can lead to water efflux from the liposomes, causing a size decrease due to osmotic dehydration.[44] The reverse case, where HSA was encapsulated in a liposome was shown to also be affected by osmotic pressure, leading to increased membrane fluidity, although no size changes were reported.[45]

The variations between samples of different ionic strength are probably a consequence of enhanced protein–liposome association at lower ionic strengths due to their longer Debye length (1.93 nm at 25 mM, to 0.78 nm at 150 mM). This produces a higher HSA surface concentration thus increasing local osmotic pressure and thus particle size decreases. Conversely, higher ionic strengths, lead to shorter Debye lengths, which screens long-range electrostatic interactions, and thus slows association (lower k_{on}) which results in smaller size and spectral changes at higher ionic strengths, as seen here.

3.2.2 Penetration phase (up to 30 minutes). The next ~30 minutes showed the largest changes in emission parameters (Fig. 4 and Fig. S6/7/8, SI) but with minimal particle size changes (Fig. 5 and Fig. S5, SI). PSD analysis using NTA

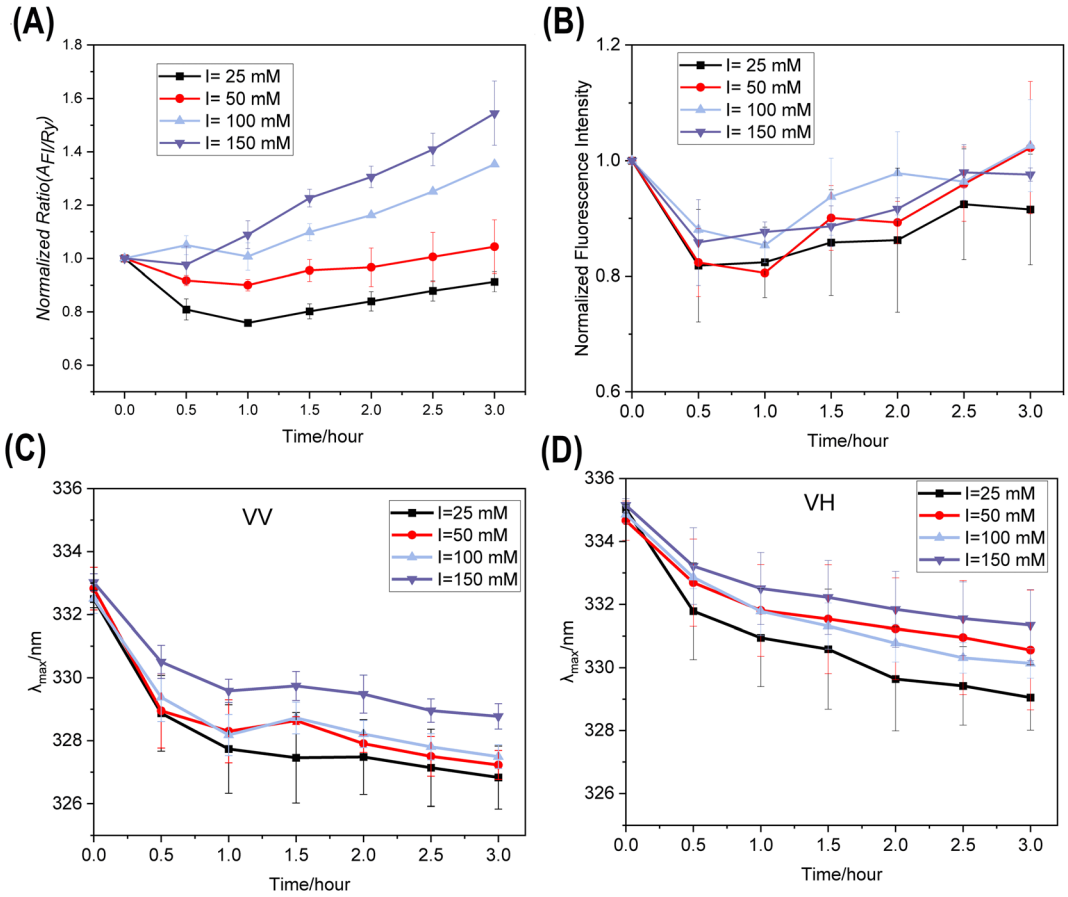

Fig. 4 Plots of protein–liposome time dependent fluorescence spectral changes *versus* time for different ionic strengths: (A) normalized $A_{FI/Ry}$ ratio (VV polarisation); (B) normalized fluorescence intensity; (C) change in emission maximum (λ_{max}), VV polarisation; (D) change in emission maximum (λ_{max}), VH polarisation. For more details, refer to the SI, Fig. S7/S8, Table S2, and Fig. S18 (statistical analysis).

(Fig. 6) also showed significant differences between the low and high ionic strength conditions at this time.

APIES measurements. By 30 minutes after mixing, the $A_{FI/Ry}$ ratio (Fig. 4A and Fig. S6A, SI) had decreased for the low ionic strength conditions (25 mM ~20% drop, and 50 mM a ~10% drop) whereas the higher ionic strengths had minimal or slight increases (see Fig. S6, SI for the high resolution plot). For all ionic strengths, the normalized fluorescence intensity decreased markedly within the first 30 minutes after mixing (Fig. 4B) accompanied by a significant time-dependent blue shift (Fig. 4C/Fig. 2D, Fig. S7A/C, and Table S2, SI). The degree of change was much greater at low ionic strengths: $\Delta\lambda_{max}$ = −3.1 ± 1.6 for 25 mM nm, compared to $\Delta\lambda_{max}$ = −1.0 ± 0.9 nm for 150 mM. Spectral shifts were attributed to environmental changes around Trp214, which is highly sensitive to polarity changes.[46,47] This blue shift indicates either a decrease in local polarity and/or an increase in hydrophobicity around Trp-214, arising from incorporation of HSA into the less polar lipid bilayer microenvironment.[40,48] The smaller blue shift at higher ionic strength was due to electrostatic screening which reduced the strength of HSA–liposome binding, and thus the degree to which the HSA penetrated the lipid layers as reported by the blue shift in the intrinsic emission. However, at lower ionic strengths weaker charge screening permitted stronger electrostatic interactions with the liposome surface, facilitating membrane penetration and thus larger blue shifts. This behaviour is consistent with the general role of ionic strength in moderating protein electrostatics and, in many protein–surface systems, reducing adsorption-driven structural perturbations.[49] There was a very small increase (caused by increased size/light scatter) in absorbance of ~1.0% after 30 minutes when compared to time zero (see Fig. S8, SI) which suggests that there was no loss in protein.

Zeta potential measurements. Both liposomes and the HSA–liposome mixtures showed a decrease in the magnitude of the ζ potential (Table 1 and Fig. S9, SI) with increasing ionic strength, reflecting compression of the electric double layer.[50] However, Zeta potential measurements of the complexes were only possible after incubation for 3 hours when we adjudged the system to be relatively stable as each sample took ~30 minutes to test in triplicate. A progressive shift in ζ potential toward less negative values was also seen for the HSA–liposome mixtures with an approximately linear dependence on ionic strength. The magnitude of the ζ potential for the mix-

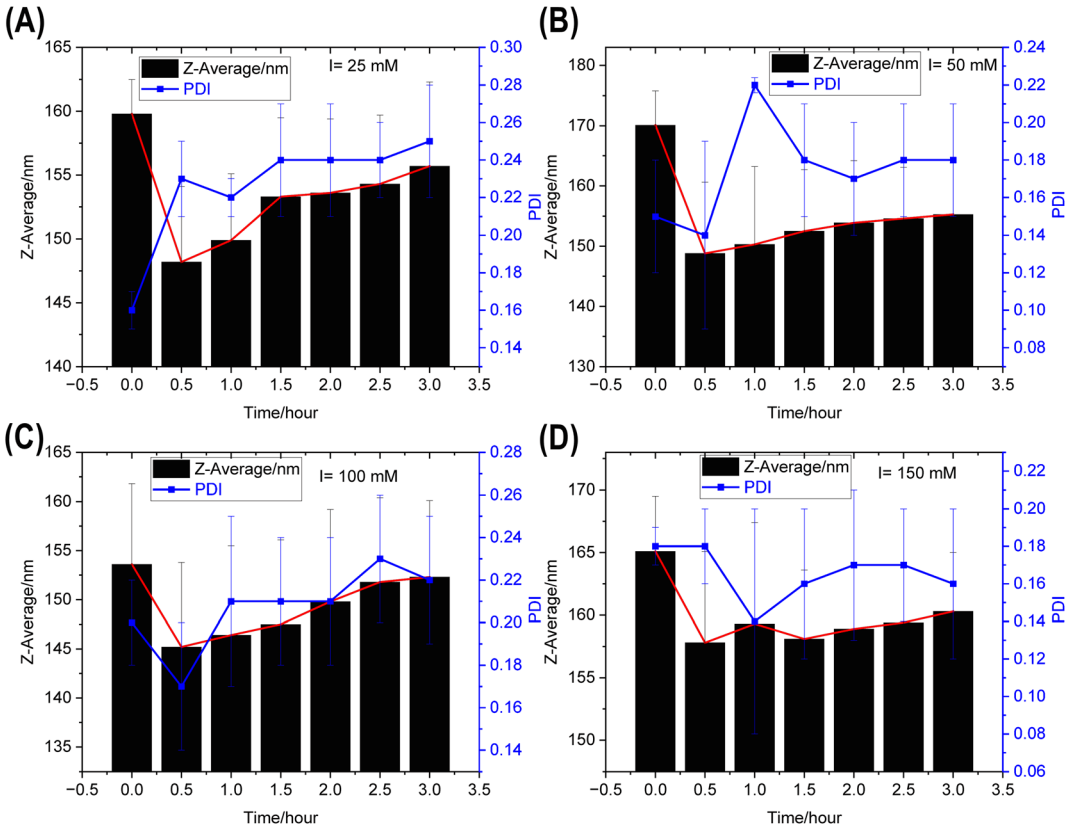

Fig. 5 Changes in average particle diameter (*Z*-average, black bars) and polydispersity index (PDI, blue line) of HSA–DMPC liposome complexes incubated at different ionic strengths 25 (A), 50 (B), 100 (C), and 150 (D) mM for up to three hours. The t = 0, 0.5, and 1.0 hour timepoints are single 10 second DLS measurements. The timepoints at 1.5 h, 2 h, 2.5 h, and 3 h are the average of 20 separate 10 s measurements. Data are presented as mean and standard deviations from three different experiments undertaken on different days. The high resolution (all 10 s individual measurements) data is shown in Fig. S5, and statistical analysis in Fig. S14/S15/S16, SI.

tures was closer to that of the liposomes and very different to that of HSA. This confirms that the measurement was representative of the HSA–liposome complexes with minimal contribution from unbound HSA. This linear dependence on ionic strength for the complexes is consistent with enhanced electrostatic screening at higher salt concentrations (see SI for further details).[51,52]

Apart from the 25 mM case, all HSA–liposome complexes had a more negative ζ potential than the free liposome. Eisermann *et al.*[53] showed that proteo-liposomes containing increasing amounts of membrane-associated proteins exhibited zeta potentials closer to neutral than protein-free liposomes, and that the magnitude of the changes correlate with the amount of protein incorporated into the membranes. Since the 25 mM case had the most negative value, we suggest that this was due to higher amounts of HSA on the surface which was similar to that reported by Weecharangsan *et al.*[54] These also agree with the fact that the largest hypsochromic shifts were observed for the lowest ionic strength which should correlate with the amount of HSA incorporated into the membrane.

Size measurements. DLS and NTA measurements of the HSA–liposome mixtures only show the liposome component and the HSA contribution was not resolved in the distribution fits. Plots of size and PDI from DLS (Fig. 5 and Fig. S5, SI) showed a clear and significant particle size decrease accompanied by a significant PdI increase (over bare liposomes) under all conditions. The detailed (every 10 s) analysis of size changes in this first 30 minutes (Fig. S5, SI) showed that nearly all the size decrease occurred in the first 200 s after which the size remained constant (50/100/150 mM) or gradually increased (by ~5 nm for 25 mM).

NTA (Fig. 6A–D and Fig. S10/S11, SI) showed that bare liposomes displayed a broad, largely single-mode distribution with a mode/mean size around ~100–180 nm, and ionic-strength changes from 25 to 150 mM produced only minor shifts in the profile (Fig. S11A, SI). After mixing with HSA the size distributions became time and ionic-strength dependent with the largest difference measured after 30 minutes. Low-ionic-strength samples (25–50 mM) had broader size distributions with a larger large-particle fraction than the high-ionic-strength samples (100–150 mM). This was also seen in the size measurements (Fig. 6E, F and Table S3, SI) with larger mean D_h at 25 mM (148 ± 3 nm) compared to 150 mM (118 ± 6 nm). It is important to note that the DLS and NTA size values are different because of the fundamental nature of the measure-

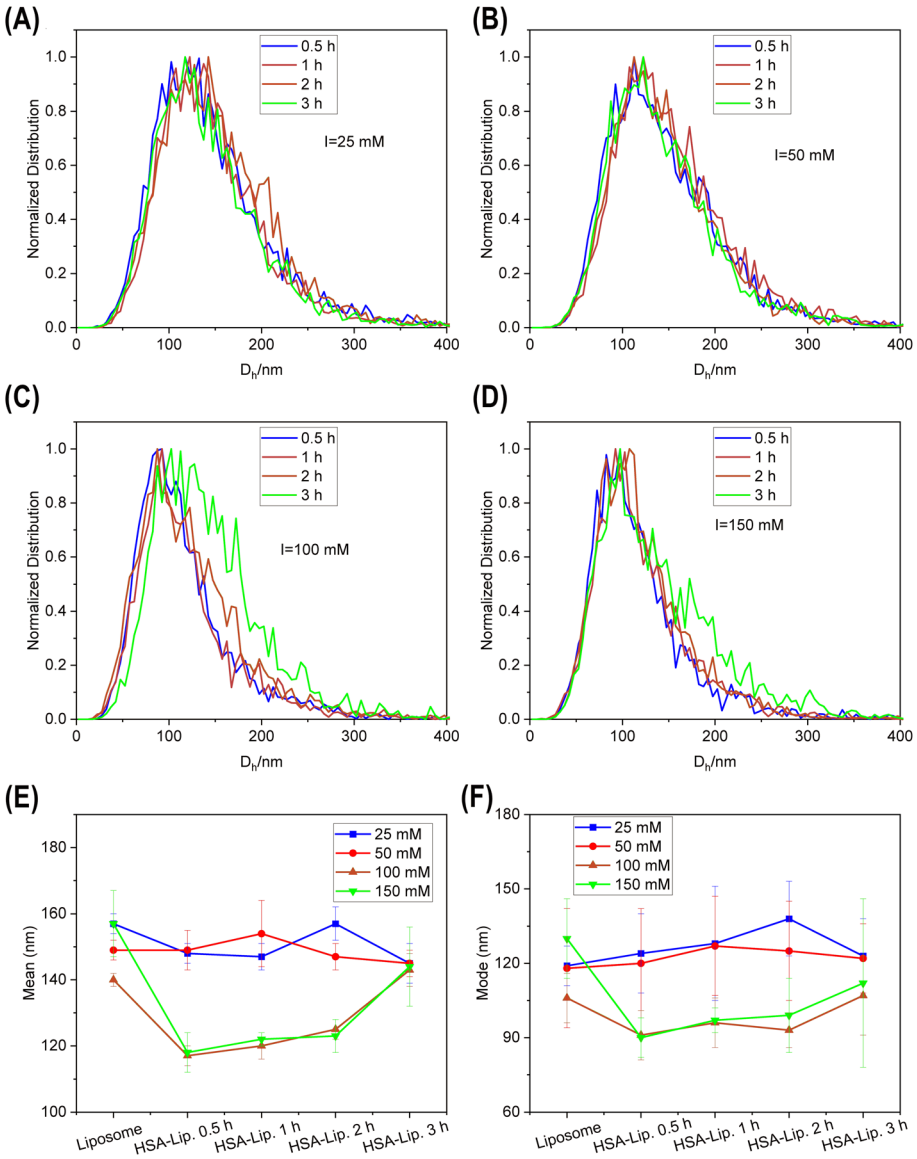

Fig. 6 NTA analysis (normalized PSD) of HSA-liposome (HSA-Lip.) interaction at different times after mixing (0.5, 1, 2, and 3 hours) under different ABC buffer ionic strengths: (A) 25 mM; (B) 50 mM; (C) 100 mM; (D) 150 mM. (E) Plot of mean diameter against time; (F) plot of mode diameter against time.

ments. The *Z*-average is the mean value from Cumulants fitting which is intensity-weighted, whereas NTA is a single-particle tracking-based mean, which more closely reflects the counted/predominant particle population.

Overall, APIES data shows that the protein–liposome interaction follows similar "bind-first, insert-later" sequences of fast surface-level associations without substantial penetration into the bilayer, followed by slower transmembrane insertion, as noted by others.[55–58] This finding was also in agreement with Kristensen, who demonstrated similar behaviour *via* fluorescence correlation spectroscopy (FCS) with serum-induced reduction in both the size and homogeneity of pegylated and non-pegylated liposomes.[59] Interestingly, they reported a much slower interaction rate, which was attributable to the much lower protein : liposome ratio and concentrations used for their FCS measurements. In contrast, Galantai reported that HSA incubation with small (D_h ~50 nm) DMPC liposomes in phosphate buffer resulted in increased particle size after 0.5 and 2.5 hours.[60] These inconsistencies highlight that the effect of HSA on liposome size is influenced many factors including lipid composition, protein–lipid interactions, experimental conditions, and measurement methods.[61,62]

3.2.3 Protein corona growth/evolution (0.5–3 h)

APIES measurements. Between 0.5 and 1 h, $A_{FI/Ry}$ ratio changed only slightly, with variations of less than 5% (Fig. 4A and Fig. S6B, SI) apart from the 150 mM solutions, however, over the next two hours, the ratio increased significantly (Fig. S19A/B, SI) for all ionic strengths. Likewise, fluorescence

intensity was relatively constant for this 30–60 minutes period, followed by a gradual increase (Fig. 4B). This change was statistically significant for 50 and 100 mM conditions, but not for the 25 and 150 mM conditions (Fig. S19C, SI). At the same time, the absorbance at 280 nm increased by 2–3% (Fig. S8, SI). Between 30–60 minutes post mixing, λ_{max} decreased less (≈1 nm) across all ionic strengths (Fig. 4C/Fig. 2D and Fig. S7B/D, SI) indicating that the rate of penetration had decreased significantly. For the next two hours the rate of change decreased further (typically ≤1 nm h^{-1}). The increase in fluorescence intensity was probably attributable to an increase in Trp quantum yield, due to reduced mobility and changing environment as HSA was incorporated into the lipid bilayer. Previously we established that the fluorescence lifetime of HSA in DMPC after 3 hours for a similar buffer was less than that of free HSA and we attributed that (and the large hypsochromic shift) as being due to a certain amount of protein unfolding and quenching.[21] However, in that study since we did not quantify intensity changes and thus confirm quenching. Here the observed increase in emission intensity with time suggests that we have a higher emission rate, and thus larger quantum yield for Trp as HSA is incorporated in the lipid bilayers. It is unlikely that the HSA penetrates into the core, as this is an aqueous domain and thus one might expect a red emission shift to be observed, which does not happen here. However, Trp photophysics and lifetimes are complex,[40,63] and further studies will be required to investigate and validate these hypotheses.

Size measurements. After the initial decrease observed during the first 30 min, HSA–liposome complex size gradually increased (by 1–5%) for all conditions and by 3 hours had reached values that were about 5–10 nm smaller than the initial liposome size (Fig. 5A–D, Table 1 and Table S3, SI). Polydispersity remained high under all conditions but was higher (~0.22–0.25) for the 25/100 mM conditions compared to the 50/150 mM samples. Interestingly, PSD differences between high and low ionic strength conditions observed by NTA, gradually disappeared (Fig. S11, SI) and was gone after 3 hours, suggesting that the system approaches a similar steady state PSD irrespective of ionic strength. This is due to electrostatic screening differences and the fact that the protein layer in the high ionic strength conditions evolves more slowly as seen by DLS/APIES and discussed above. However, we do have to be cautious here as the NTA measurements were made on very dilute samples and thus any reversible associations/aggregates present in the more concentrated reaction mixtures may have disassociated.

We also found that changes in the normalized $A_{FI/Ry}$ ratio and *Z*-Ave. correlated linearly (Fig. S12A, SI) for all ionic strength conditions, although the error in size measurements was very large. Whereas normalized $A_{FI/Ry}$ ratio and mean size by NTA (Fig. S12B, SI) showed a strong size trend only for the two higher ionic strengths. The differences could be attributed to a number of factors: first, the $A_{FI/Ry}$ ratio uses the Rayleigh–Mie light scatter signal, which is mostly Mie (particle) scattered light in this system, and this is the same physical phenomena that is measured in DLS.[64] Thus, they follow the same intensity-size trends, and a linear correlation is expected as long as the emission does not change significantly due to other factors. In contrast, the NTA mean value is a number-based measurement and thus independent of the scattered light intensity to particle size relationship.[65] Second, NTA data was collected from diluted samples and thus the PSD is probably different from the undiluted samples analysed by DLS.

4. Conclusions

Our original hypothesis was that the initial interaction between HSA and liposomes was very fast[21] and thus required a faster measurement method to properly monitor the process. A multichannel based fluorometer which simultaneously measures absorbance, like the Aqualog from Horiba used here, provided acceptable hardware capability and timing resolution (~1 s), missing from standard scanning-based spectrometers. Thus, APIES approach where one simultaneously measures absorbance, Rayleigh–Mie (elastic) scattering, and intrinsic fluorescence emission, with one second temporal resolution, provides real time insights into interaction processes over extended periods.

APIES showed with high temporal resolution that the interaction of HSA with liposomes to form a mono-protein corona was a three-phase process: first a fast surface adsorption of HSA with a simultaneous osmotic driven, small reduction in liposome size (0–200 seconds); second a reorganization phase in which the adsorbed HSA penetrates the lipid bilayer (3–30 minutes); and finally an annealing phase in which we see a gradual increase in particle size along with further protein penetration (>30 minutes). APIES characterized the first phase by a constant absorbance (*i.e.* no protein loss), small reductions reduction in emission intensity and $A_{FI/Ry}$ ratio, with no significant spectral shifts. The second phase was evidenced by constant absorbance, minimal changes in $A_{FI/Ry}$ ratio, but relatively large blue shifts (indicative of tryptophan environment changes[66]). The final phase displayed constant absorbance, gradual increase in $A_{FI/Ry}$ ratio and fluorescence intensity with minimal change in the emission maximum.

In terms of assessing ionic strength effects, APIES clearly shows the dual role of electrostatic screening and protein–lipid binding in governing protein corona formation, in agreement with previous reports on the sensitivity of protein–nanoparticle interactions to ionic strength and buffer conditions.[67,68] Electrostatic screening modulates adsorption: at low ionic strength, screening is weak, and thus binding is facilitated, whereas at higher ionic strength charge effects are strongly screened, reducing the electrostatic driving force, and slowing adsorption.[51–54] All these effects were seen in the changes in the simultaneously measured APIES parameters: absorbance yielding solution protein concentration, the $A_{FI/Ry}$ ratio showing particle size changes, emission maxima reporting degree of membrane penetration, fluorescence intensity showing both solution concentration and fluorophore environ-

ment. Finally, the normalized $A_{FI/Ry}$ ratio correlated linearly with changes in D_h (Z-average) under all conditions, providing a quasi-quantitative size model to track size changes.

The statistical significance of changes in measured spectral parameters and DLS obtained size data with time and ionic strength were evaluated *via* two-way ANOVA (section S1.12 SI). In general, APIES outperforms DLS in generating statistically significant measurement parameters ($A_{FI/Ry}$ ratios, emission intensities, and λ_{max}) with which one can monitor protein–liposomes interactions during the different phases (Table S4, SI). Thus, in this experimental configuration, one can easily follow trends and differences, however, extraction of quantitative kinetic data would require further optimization to improve signal-to-noise ratios, reduce measurement error, and increase statistical significance. Here, however, the biggest source of error between replicate measurements was the intrinsic variability of the liposomes themselves which were manually prepared fresh for each experiment. Under such circumstances, extracting quantitative binding kinetic data will require higher replicate numbers (9 or more) and more consistent liposome manufacture.

Size only characterization methods, DLS and NTA, provided much less information about the binding-interaction processes. NTA was better at resolving the PSD, and showed differences between high and low ionic strengths, but provided little else about the interaction process. ζ-Potential measurements, reflecting surface charge distribution and the state of the interfacial double layer, does show how ionic strength affected protein–liposome association, but this was an indirect measure of binding.[53,54] Compared to more complex FCS based analysis[59] which requires dilution and much more involved experimental procedures, APIES can be implemented more easily, is label free, on more clinically relevant concentrations, with higher time resolution. Although the capital costs of the fluorescence spectrometer used here may be similar to NTA or advanced, multiangle DLS systems, the unit test cost is essentially negligible as the cuvette is reusable, there are no expensive reagents or consumables, and the lamp source is typically very-long lived and relatively inexpensive to replace.

To conclude, APIES provides a new, fast, non-invasive, and robust method for monitoring protein liposome (or nanoparticle) interactions with a temporal resolution of ~1 s that only requires simple data analysis that can be executed using standard spreadsheets. The APIES approach can thus form the basis of a cost-effective *in vitro* test method for screening nanoparticle formulations in terms of their interaction with proteins.

Author contributions

Huajie F. Wang: conceptualization, designed and performed the experiments, analysed the data, prepared all the figures, wrote, and edited the manuscript. Alan Ryder: conceptualization, supervision, resource provision, wrote and edited the manuscript.

Conflicts of interest

Horiba Scientific (NJ, USA) are a collaborator of the NBL and provided the Aqualog spectrometer used in these studies. They were not involved in any way with the research design, implementation, analysis of the results or writing of the paper. The authors declare that there are no other conflicts of interest.

Data availability

Data for this article, including tables of DLS data, zeta potential plots, 2D emission spectra, and absorbance values are freely available in Excel file format on the Zenodo repository on the NBL lab page: https://zenodo.org/communities/nano-bio-lab/. The DOI is 10.5281/zenodo.19827043.

Supplementary information (SI): additional experimental and statistical analysis data. See DOI: https://doi.org/10.1039/d6nr00519e.

Acknowledgements

This publication has emanated from research supported in part by a China Scholarship Council grant to HW (No. 202308310150) and the University of Galway. We thank Horiba (Piscataway, NJ, USA) for the loan of the Aqualog instrumentation used in this study.

References

1 S. Mojarad-Jabali, Y. Fatahi and R. Dinarvand, *Eur. J. Pharm. Sci.*, 2025, **212**, 107166.
2 L. Vroman, *Nature*, 1962, **196**, 476–477.
3 F. Giulimondi, L. Digiacomo, D. Pozzi, S. Palchetti, E. Vulpis, A. L. Capriotti, R. Z. Chiozzi, A. Laganà, H. Amenitsch, L. Masuelli, G. Peruzzi, M. Mahmoudi, I. Screpanti, A. Zingoni and G. Caracciolo, *Nat. Commun.*, 2019, **10**, 3686.
4 J. Sabín, G. Prieto, J. M. Ruso, P. V. Messina, F. J. Salgado, M. Nogueira, M. Costas and F. Sarmiento, *J. Phys. Chem. B*, 2009, **113**, 1655–1661.
5 W. Wang, Z. Huang, Y. Li, W. Wang, J. Shi, F. Fu, Y. Huang, X. Pan and C. Wu, *Acta Pharm. Sin. B*, 2021, **11**, 1030–1046.
6 P. Bełdowski, M. Przybyłek, P. Raczyński, A. Dedinaite, K. Górny, F. Wieland, Z. Dendzik, A. Sionkowska and P. M. Claesson, *Int. J. Mol. Sci.*, 2021, **22**, 12360.
7 T. Ohyashiki, M. Taka and T. Mohri, *J. Biol. Chem.*, 1985, **260**, 6857–6861.
8 J. U. De Mel, S. Gupta, R. M. Perera, L. Ngo, P. Zolnierczuk, M. Bleuel, S. V. Pingali and G. J. Schneider, *Langmuir*, 2020, **36**, 9356–9367.
9 L. Guo, R. L. Hamilton, J. Goerke, J. N. Weinstein and R. J. Havel, *J. Lipid Res.*, 1980, **21**, 993–1003.

10 S. Pande, *Artif. Cells. Nanomed. Biotechnol.*, 2023, **51**, 428–440.
11 V. Nele, F. D'Aria, V. Campani, T. Silvestri, M. Biondi, C. Giancola and G. De Rosa, *J. Liposome Res.*, 2024, **34**, 88–96.
12 A. Aguilera-Garrido, T. del Castillo-Santaella, Y. Yang, F. Galisteo-González, M. J. Gálvez-Ruiz, J. A. Molina-Bolívar, J. A. Holgado-Terriza, M. Á. Cabrerizo-Vílchez and J. Maldonado-Valderrama, *Adv. Colloid Interface Sci.*, 2021, **290**, 102365.
13 M. Hadjidemetriou, Z. Al-Ahmady and K. Kostarelos, *Nanoscale*, 2016, **8**, 6948–6957.
14 R. B. Gennis and A. Jonas, *Annu. Rev. Biophys. Bioeng.*, 1977, **6**, 195–238.
15 N. Voskoboynikova, E. G. Margheritis, F. Kodde, M. Rademacher, M. Schowe, A. Budke-Gieseking, O.-E. Psathaki, H.-J. Steinhoff and K. Cosentino, *Biochim. Biophys. Acta, Biomembr.*, 2021, **1863**, 183588.
16 B. J. Berne and R. Pecora, *Dynamic light scattering: with applications to chemistry, biology, and physics*, Courier Corporation, 2000.
17 S. K. Filippov, R. Khusnutdinov, A. Murmiliuk, W. Inam, L. Y. Zakharova, H. Zhang and V. V. Khutoryanskiy, *Mater. Horiz.*, 2023, **10**, 5354–5370.
18 N. Van der Sanden, R. A. Paun, M. Y. Yitayew, O. Boyadjian and M. Tabrizian, *Nanoscale Adv.*, 2025, **7**, 169–184.
19 F. Fu, D. Crespy, K. Landfester and S. Jiang, *Chem. Soc. Rev.*, 2024, **53**, 10827–10851.
20 B. Hoseini, M. R. Jaafari, A. Golabpour, A. A. Momtazi-Borojeni, M. Karimi and S. Eslami, *Sci. Rep.*, 2023, **13**, 18012.
21 F. Gordon, Y. Casamayou-Boucau and A. G. Ryder, *Colloids Surf., B*, 2022, **211**, 112310.
22 M. Steiner-Browne, S. Elcoroaristizabal, Y. Casamayou-Boucau and A. G. Ryder, *Chemom. Intell. Lab. Syst.*, 2019, **185**, 1–11.
23 B. O. Boateng, S. Elcoroaristizabal and A. G. Ryder, *Biotechnol. Bioeng.*, 2021, **118**, 1805–1817.
24 A. Jain and S. K. Jain, *Chem. Phys. Lipids*, 2016, **201**, 28–40.
25 B. O. Boateng and A. G. Ryder, *Anal. Chim. Acta*, 2026, **1383**, 344894.
26 S. Bhattacharjee, *J. Controlled Release*, 2016, **235**, 337–351.
27 Y. Casamayou-Boucau and A. G. Ryder, *Anal. Chim. Acta*, 2020, **1138**, 18–29.
28 Y. Casamayou-Boucau and A. G. Ryder, *Methods Appl. Fluoresc.*, 2017, **5**, 037001.
29 J. D. Zang and A. G. Ryder, *Viral Inactivation Process Monitoring by APIES (Absorbance, Polarized Intrinsic Emission, and light Scattering): simultaneous protein aggregation, concentration, and stability analysis,* 2026, submitted.
30 R. A. Dragovic, C. Gardiner, A. S. Brooks, D. S. Tannetta, D. J. P. Ferguson, P. Hole, B. Carr, C. W. G. Redman, A. L. Harris, P. J. Dobson, P. Harrison and I. L. Sargent, *Nanomedicine*, 2011, **7**, 780–788.
31 D. M. Jameson and J. A. Ross, *Chem. Rev.*, 2010, **110**, 2685–2708.
32 J. N. Israelachvili, *Intermolecular and surface forces*, Academic press, 2011.
33 Y.-W. Choi, S. Lee, K. Kim, P. S. Russo and D. Sohn, *J. Colloid Interface Sci.*, 2007, **313**, 469–475.
34 K. Fischer and M. Schmidt, *Biomaterials*, 2016, **98**, 79–91.
35 D. J. A. Crommelin, *J. Pharm. Sci.*, 1984, **73**, 1559–1563.
36 S. Hupfeld, H. H. Moen, D. Ausbacher, H. Haas and M. Brandl, *Chem. Phys. Lipids*, 2010, **163**, 141–147.
37 X. Wang, C. J. Swing, T. Feng, S. Xia, J. Yu and X. Zhang, *J. Dispersion Sci. Technol.*, 2020, **41**, 1568–1575.
38 C. Chaix, E. Pacard, A. Elaïssari, J.-F. Hilaire and C. Pichot, *Colloids Surf., B*, 2003, **29**, 39–52.
39 S. Garcia-Manyes, G. Oncins and F. Sanz, *Biophys. J.*, 2005, **89**, 1812–1826.
40 J. R. Lakowicz, *Principles of fluorescence spectroscopy*, Springer, 2006.
41 A. Small, S. Hong and D. Pine, *J. Polym. Sci., Part B: Polym. Phys.*, 2005, **43**, 3534–3548.
42 T. Sanvito, P. Bigini, M. V. Cavanna, F. Fiordaliso, M. B. Violatto, L. Talamini, M. Salmona, P. Milani and M. A. C. Potenza, *Nanomedicine*, 2017, **13**, 2597–2603.
43 M. Dolci, Y. Wang, S. W. Nooteboom, P. E. D. Soto Rodríguez, S. Sánchez, L. Albertazzi and P. Zijlstra, *ACS Nano*, 2023, **17**, 20167–20178.
44 J. Wolfram, K. Suri, Y. Yang, J. Shen, C. Celia, M. Fresta, Y. Zhao, H. Shen and M. Ferrari, *Colloids Surf., B*, 2014, **114**, 294–300.
45 T. Kure and H. Sakai, *Langmuir*, 2017, **33**, 1533–1540.
46 X. M. He and D. C. Carter, *Nature*, 1992, **358**, 209–215.
47 A. Chattopadhyay, S. S. Rawat, D. A. Kelkar, S. Ray and A. Chakrabarti, *Protein Sci.*, 2003, **12**, 2389–2403.
48 J. T. Vivian and P. R. Callis, *Biophys. J.*, 2001, **80**, 2093–2109.
49 H. X. Zhou and X. Pang, *Chem. Rev.*, 2018, **118**, 1691–1741.
50 A. T. Poortinga, R. Bos, W. Norde and H. J. Busscher, *Surf. Sci. Rep.*, 2002, **47**, 1–32.
51 H.-X. Zhou and X. Pang, *Chem. Rev.*, 2018, **118**, 1691–1741.
52 P. Foteini, N. Pippa, N. Naziris and C. Demetzos, *J. Liposome Res.*, 2019, **29**, 313–321.
53 J. Eisermann, J. J. Wright, J. D. Wilton-Ely, J. Hirst and M. M. Roessler, *RSC Chem. Biol.*, 2023, **4**, 386–398.
54 W. Weecharangsan, B. Yu, Y. Zheng, S. Liu, J. X. Pang, L. J. Lee, G. Marcucci and R. J. Lee, *Mol. Pharm.*, 2009, **6**, 1848–1855.
55 O. A. Andreev, A. G. Karabadzhak, D. Weerakkody, G. O. Andreev, D. M. Engelman and Y. K. Reshetnyak, *Proc. Natl. Acad. Sci. U. S. A.*, 2010, **107**, 4081–4086.
56 Y. K. Reshetnyak, O. A. Andreev, M. Segala, V. S. Markin and D. M. Engelman, *Proc. Natl. Acad. Sci. U. S. A.*, 2008, **105**, 15340–15345.
57 R. Thakur, A. Das and A. Chakraborty, *RSC Adv.*, 2014, **4**, 14335–14347.
58 W. C. Wimley and S. H. White, *Nat. Struct. Biol.*, 1996, **3**, 842–848.
59 K. Kristensen, A. J. Urquhart, E. Thormann and T. L. Andresen, *Nanoscale*, 2016, **8**, 19726–19736.

60 R. Galántai and I. Bárdos-Nagy, *Int. J. Pharm.*, 2000, **195**, 207–218.
61 H. Nsairat, D. Khater, U. Sayed, F. Odeh, A. Al Bawab and W. Alshaer, *Heliyon*, 2022, **8**, e09394.
62 R. M. Amărandi, A. Neamțu, R. I. Ştiufiuc, L. Marin and B. Drăgoi, *ACS Omega*, 2024, **9**, 17903–17918.
63 M. Amiri, K. Jankeje and J. R. Albani, *J. Fluoresc.*, 2010, **20**, 651–656.
64 B. J. Berne and R. Pecora, *Dynamic Light Scattering*, Dover Publications Inc., Mineola, N.Y., 2000.
65 C. M. Maguire, M. Rosslein, P. Wick and A. Prina-Mello, *Sci. Technol. Adv. Mater.*, 2018, **19**, 732–745.
66 K. M. Sanchez, G. Kang, B. Wu and J. E. Kim, *Biophys. J.*, 2011, **100**, 2121–2130.
67 X. Wang, S. Zhang, Y. Xu, X. Zhao and X. Guo, *Langmuir*, 2018, **34**, 8264–8273.
68 Y. Bae and X. Liu, *Environ. Pollut.*, 2024, **346**, 123552.